UC Irvine

UC Irvine Previously Published Works

Title

Dynamic modeling of Hydrogen SOFC/GT powered Aircraft with integration analysis

Permalink

https://escholarship.org/uc/item/0c20q9p4

Authors

Alsamri, Khaled

Rezaei, Sajjad

Chung, Vanessa

et al.

Publication Date

2024-01-08

DOI

10.2514/6.2024-1532

Peer reviewed

eScholarship.org Powered by the California Digital Library
University of California

Dynamic modeling of Hydrogen SOFC/GT powered Aircraft with integration analysis

Khaled Alsamri[1], Sajjad Rezaei[2], Vanessa Chung[3] , Jacqueline Huynh[4] and Jack Brouwer[5]

University of California Irvine, 4200 Engineering Gateway, Irvine, CA, 92697

This paper aims to advance the green transition of the aviation industry by introducing a dynamic modeling approach for the integration of hydrogen solid oxide fuel cells (SOFCs) and gas turbines (GTs) in aircraft propulsion. Despite the significant potential for emission reduction and improved fuel efficiency, the adoption of the SOFC/GT system in aviation is impeded by many factors, which include a lack of understanding of dynamic performance under diverse flight conditions. Through a comprehensive approach that leverages the STRIDES dynamic modeling program, this paper presents an analysis of the dynamic response and electrochemical characteristics of the system under the varying power demands of a flight. The designed system achieves efficiency of 71.4% and a power output of 1.29MW. The methodology also emphasizes the complexities of flight conditions and potential areas for system optimization and improvement. The study, with a focus on the rapid response of the SOFC/GT system operated in a representative Cessna S550 Citation S/II aircraft flight under dynamic conditions, paves the way for the broader adoption of this technology, contributing to the mitigation of the environmental impacts of aviation.

[1] Graduate Student, Department of Mechanical and Aerospace Engineering at the University of California Irvine,
4200 Engineering Gateway, Irvine CA, 92697, and AIAA Student Member.
[2] Graduate Student, Department of Chemical & Biomolecular Engineering at the University of California, Irvine, USA
[3] Graduate Student, Department of Mechanical and Aerospace Engineering at the University of California Irvine,
4200 Engineering Gateway, Irvine CA, 92697, and AIAA Student Member.
[4] Assistant Professor, Department of Mechanical and Aerospace Engineering at the University of California Irvine,
4200 Engineering Gateway, Irvine CA, 92697, and AIAA Member.
[5] Director of Advanced Power and Energy Program, Department of Mechanical and Aerospace Engineering, University of California Irvine/4200 Engineering Gateway Irvine CA 92697, and AIAA Member.

I. Nomenclature

- $V = Cell\ voltage\ (V)$
- $v_{rev} = Standard\ electrode\ potential\ (V)$
- $R = Universal\ gas\ constant\ (J/(mol \cdot K))$
- $T = Temperature\ (K)$
- $n = Number\ of\ electrons\ transferred$
- $F = Faraday's\ constant\ (C/mol)$
- $\rho = Density\ (kg/m^3)$
- $P_{O_2} = Partial\ pressure\ of\ O_2\ (atm)$
- $P_{H_2} = Partial\ pressure\ of\ H_2\ (atm)$
- $P_{H_2O} = Partial\ pressure\ of\ H_2O\ (atm)$
- $P_{stack} = Stack\ power\ (kW)$
- $\eta = Overpotential\ (mV)$
- $j = Current\ (A)$
- $j_0 = Exchange\ current\ density\ (A/m^2)$
- $C_P = Constant\ pressure\ specific\ heat\ (kJ/kg \cdot K)$
- $C_V = Constant\ volume\ specific\ heat\ (kJ/kg \cdot K)$
- $D_h = Hydraulic\ diameter\ (m)$
- $G = Gibbs\ free\ energy\ (kJ)$
- $h = Specific\ enthalpy\ (kJ/mol)$
- $h_c = Convective\ heat\ transfer\ coefficient\ (W/m^2.K)$
- $\dot{m} = Mass\ flow\ rate\ (kg/s)$
- $\dot{n} = Molar\ flow\ rate\ (kmol/s)$
- $\eta = Efficiency\ /overpotential$
- $N_{Flow} = Normalized\ mass\ flow$
- $N_{RPM} = Normalized\ shaft\ speed$
- $Nu = Nusselt\ number$
- $PR = Pressure\ ratio$
- $k = Thermal\ conductivity\ (W/m \cdot K)$
- $U_{fuel} = Fuel\ utilization$
- $Q = Heat\ transferred\ (kJ)$
- $W = Work\ (kJ)$
- $m_{\text{air,compressor}} = Air\ entering\ the\ Compressor$
- $m_{air_{SOFC,}} = Air\ entering\ the\ SOFC$
- $m_{\text{steam}} = Steam\ flow\ towards\ theSOFC$
- $m_{\text{fuel,pump}} = Fuel\ flowt\ owards\ the\ Fuel\ Pump$
- $m_{\text{fuel,combustor}} = Fuel\ flow\ directly\ to\ the\ Combustor$
- $m_{\text{combustor}} = Combined\ flowentering\ the\ Combustor\ (fromSOFCandFuel)$
- $m_{\text{turbines}} = Flow\ from\ the\ Combustor\ to\ the\ Turbines$
- $m_{\text{exhaust}} = Exhaust\ flow\ from\ Turbines$
- $m_{\text{air,fuelheater}} = Air\ entering\ the\ FuelHeater$
- $m_{\text{loss}} = Heatloss\ from\ the\ Fuel\ Heater$
- $R = Range\ (m)$
- $g = Gravitational\ force\ \left(\frac{m}{s^2}\right)$
- $w_{fuel} = Weight\ of\ fuel\ (kg)$
- $\eta = \text{Pr}\,o\,pulsion\ system\ efficiency$

- $h_f = Fuel\ specific\ energy$
- $\frac{L}{D} = Aerodynamic\ efficiency$
- $T = Thrust\ [N]$
- $\rho = Density\ of\ air\ \left(\frac{kg}{m^3}\right)$
- $v = Velocity\ \left(\frac{m}{s}\right)$
- $D = Drag\ (N)$
- $S_{ref} = Wing\ reference\ area\ (m^2)$
- $C_{D_o} = Profile\ drag\ coefficient$
- $C_{D_c} = Compressibility\ drag\ coefficient$
- $C_{D_{gear}} = Landing\ gear\ drag\ coefficient$
- $C_{D_I} = Induced\ drag\ coefficient$
- $\gamma = C\lim b\ angle\ (°)$
- $RPM = rotations\ per\ minute$
- $T_{cath_{in}} = Cathode\ inlet\ temperature$
- $T_{anode_{in}} = Anode\ inlet\ temperature$

II. Introduction

Aviation contributes around 2.5% of global carbon dioxide emissions, and this figure is expected to grow significantly with the projected increase in air travel [1][2]. Therefore, a transition towards a greener and more sustainable aviation industry is one of the most urgent challenges that the global community must address. A promising pathway for achieving this could be the use of solid oxide fuel cell (SOFC) systems in conjunction with gas turbines (GTs), powered by hydrogen, for aircraft. SOFCs are electrochemical devices which include separated fuel and air electrodes with an oxygen ion conducting electrolyte in between providing low carbonaceous, NOx, and SOx emissions, with high efficiency (>50%), modularity, and fuel flexibility [2]. Furthermore, regarding efficiency, SOFC/GT systems have demonstrated efficiencies of up to 75% in stationary applications, compared to the current aircraft gas turbine engines that hover around 40-42% under optimal flight conditions [3]. The retrofitting and integration of such systems into modern aircraft is showcased in [4] where the system is shown to be feasible in the business jet category, being one of the more challenging categories to transform. Despite these appealing attributes, its adoption in aviation has been hindered due to many factors, including low technology readiness level (TRL) compared to other fuel cells, batteries, or hydrogen combustion, a brittle materials set, and a relatively low power density compared to gas turbines. The adoption has also been partially hindered due to a lack of comprehensive understanding of the dynamic performance characteristics in aviation applications to verify its operational viability under the wide range of dynamic and harsh conditions encountered during flight.

The U.S. Federal Aviation Regulations, such as 14 CFR Parts 23.67, 25.111, 25.121, 25.149, 25.207, and 25.251, define key performance and safety benchmarks for aircraft. These regulations mandate a minimum 1.5% climb gradient for single-engine aircraft with an inoperative engine, a 35-foot minimum takeoff path clearance for two-engine airplanes, engine-out climb gradients of

2.7% en-route and 2.4% during landing configurations and establish minimum control speeds and stall warnings [5]. They also specify vibration and buffet test requirements, crucial for assessing aircraft structure, powertrain systems, and safety. These metrics are vital to look out for when retrofitting and modeling to simulate retrofitted aircraft capabilities.

Dynamic models for SOFC/GT have been developed and tested through a modeling framework reported by Rossi et al. [6], and via a pressurized ground simulation by Roberts & Brouwer [7], which could portray the system behavior at different pressures/altitudes of flight conditions. Mueller et al. [8] also demonstrated a control design strategy for a bottoming SOFC/GT system. Pourabedin & Ommi employed a dynamic modeling approach to study the behavior of an auxiliary power unit (APU) system for a regional jet aircraft comprising a planar SOFC system with a jet fuel external reformer [9]. This modeling study illustrated that any abrupt changes in the load may lead to the most substantial losses in activation and ohmic voltage during the engine start phase, with the lowest losses happening during the cruising phase. However, the responses of concentration polarization and double-layer charging were shown to be opposite. Using a one-dimensional dynamic model, Chakravarthula studied a SOFC (with microtubular structure)/GT system performance for aviation applications [10]. This work demonstrated that, through a simple enthalpy comparison, an SOFC/GT system can achieve approximately 24% higher efficiency than a conventional turbo-generator system. Moreover, it was shown that combining SOFC with the gas turbine not only reduces the size of the gas turbine owing to reduced mass flow rates and compression pressure ratios, lowering weight and drag, but also simplifies and reduces the cost of turbine manufacture with lower intake temperatures.
The integration of hydrogen-powered SOFC/GT systems into aircraft represents a significant step towards sustainable aviation, but requires careful consideration of propulsion system dynamics to meet stringent safety and performance standards.

The rapid throttle time of conventional aircraft engines needs a 5-10 second transition from idle to maximum power, assuring compliance with safety and flying quality criteria [11,12]. This quick response contrasts with the slower dynamic response of fuel cells, where power output adjustments are constrained by the time needed to create ion concentration gradients. This duration can range from several seconds to minutes, influenced by the fuel cell type and operating scenarios. To ensure the hybrid SOFC-GT system viability within these parameters, a control strategy tailored to its dynamic stability is imperative. Previous research indicates that SOFC systems have evolved to feature dynamic stability, with transient response time now aligning closer to traditional power systems, enhancing the SOFC-GT system performance potential. Such advancements reinforce SOFC technology prospects for efficient power generation in aviation. For instance, Zhang et al. [13] reported a rapid turndown response of 48.4% in just 10 seconds for a 373.6 kW system. The disparity in response times becomes even more pronounced when considering larger transitions. Ahrned et al. [14] observed a significant turndown of 66.2% over approximately 40,000 seconds for a 3,310-kW system. Similarly, ramp-up times vary, with Ferrari et al. [15] noting a 20.1% increase in load within 900 seconds for a 278-kW system. On the larger scale, a study by McLarty et al. [16] showed a 10% load increase for a 100 MW system over 120 seconds, suggesting that while smaller systems demonstrate remarkable responsiveness, there is a significant lag in the reaction times of MW-scale systems. The data implies a need for advancement in the response capabilities of larger power systems to match the agility seen in kW-scale counterparts.

This research strives to fill this significant gap in the literature. The dynamic behavior of the hydrogen-powered SOFC/GT system in an aviation context remains relatively unexplored, forming the basis of our investigation. We present a novel approach to dynamic modeling of a representative retrofitted SOFC/GT powered Cessna S550 Citation S/II, meticulously accounting for the intricate complexities of flight conditions. This study is critical as the robustness of the SOFC/GT system under dynamic conditions is the key to ensuring the system safety, reliability, and commercial viability. By examining and validating the response of the SOFC/GT system to these conditions, we pave the way for the broader adoption of this technology, contributing to the global efforts in mitigating the environmental impact of aviation.

III.Methodology

The methodology for modeling Solid Oxide Fuel Cell (SOFC)/Gas Turbine (GT) powered aircraft primarily utilizes EAGERS and STRIDES, dynamic modeling tools within MATLAB. EAGERS, developed by Washington State University's Clean Energy Systems Integration Lab, is an open-source platform recognized for its extensive capabilities in analyzing and optimizing various energy systems [17]. Its scalable, modular design is ideal for designing, simulating, and controlling district energy systems. STRIDES complements EAGERS by facilitating non-linear simulation of energy system components, such as heat exchangers, batteries, inverters, and fuel cells, which can be integrated into larger systems and networks. This tool's strength lies in its ability to perform high-fidelity simulations using both detailed physical models and simplified reduced-order models, with local controllers for each component, enhancing its applicability to aircraft powertrain simulations.

The primary focus of the model is the dynamic response of the system to varying power demands, alongside a comprehensive analysis of its electrochemical characteristics. The model will be configured using the EAGERS platform to represent the SOFC/GT system and its components accurately, followed by the definition of the governing equations and system constraints. The research emphasizes investigating the complex interaction between the dynamic behavior of the power system and the underlying electrochemical processes within the SOFC. This synergistic modeling approach aims to identify potential areas for system optimization and improvement.

For an effective dynamics model of a SOFC/GT system, it is essential to incorporate specific thermochemical conditions, SOFC properties, GT transfer functions, and geometrical component specifications. These conditions, encompassing input, output, and internal system flows, can be figured out using built in Fuel-cell stack code under both nominal and partial loads. Key SOFC characteristics such as the polarization curve, cell count, operating temperature, and fuel type are also input, alongside the GT transfer function at varied loads. The model also requires precise controls for regulating fuel and air supply, temperature, and potentially load adjustments on the GT, ensuring a realistic simulation.

The simplified framework In Figure 1, we present an integrative framework for the dynamic modeling of a Solid Oxide Fuel Cell (SOFC) as part of an aircraft power system. The model emphasis the initialization process with the SOFC operating conditions, including temperature, flow rates, fuel utilization, and an initialization of each component in isolation. This modular

approach facilitates targeted optimizations and adjustments, ensuring each component reaches a steady operational state before integration into the larger system.

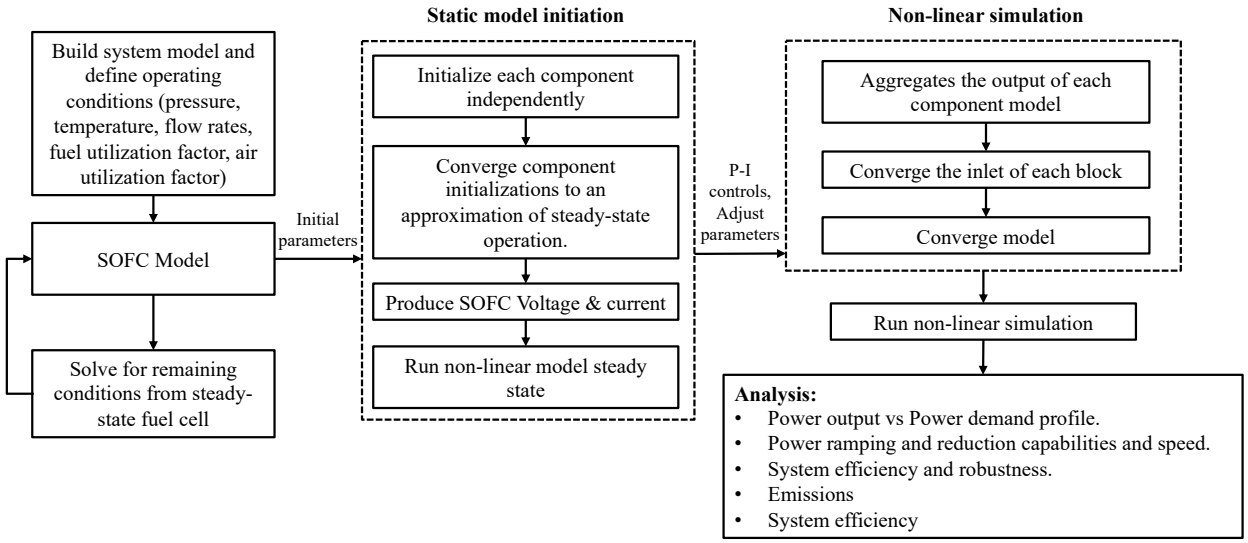

Figure 1: Flowchart of SOFC/GT System Modeling and Analysis Process

Once the system is constructed and initial parameters (IP) are established, the Solid Oxide Fuel Cell (SOFC) model becomes pivotal for resolving the remaining conditions from a steady-state perspective of the fuel cell. With the system assembled and initial parameter estimates in place, the state-state model initiates by separately initializing components and then converging these initializations to approximate a steady state. Subsequently, it runs the non-linear model over this steady state for a 24-hour period. After achieving a steady state, Proportional-Integral (PI) controls are fine-tuned, allowing the model to respond to a non-linear profile. The outputs of each component are aggregated, and the inlets of each component block are combined before the model converges and reacts to the power demand profile. This convergence enables a comprehensive analysis of the system's behavior over time. The analysis focuses on power output relative to power demand profiles, which reflects the system's capacity to meet the aircraft's operational requirements. Moreover, the model rigorously examines the capabilities for power ramping and reduction, which are crucial for aircraft systems that need to rapidly adapt to fluctuating power requirements.

The model shown in in Figure 2, depicting the Powertrain Solid Oxide Fuel Cell (SOFC) hybrid setup for Medium-Range and Long-Range aircraft, will be primarily employed. This powertrain was designed in our previous paper but received a few optimizations [18]. The design will be realized and scrutinized via the modeling and simulation in STRIDES. The cell/stack model, governed by equations (1-22), encompasses an electrochemical model and energy balance of the positive-electrolyte-negative electrode (PEN), as well as the energy balance of fuel and air plates, and fuel airflow in channels. A comprehensive dynamic mass balance equation for the entire system is established. The core of the system design is the heat and power production by the quasi-3D SOFC model, wherein the fuel cell is integrated into a topping heating cycle. An oxidizer raises the exit temperature for use in a recuperator, which increases compressed air inlet temperatures.

The resulting heated flow drives a turbine that mechanically operates the compressor, maintaining a pressurized system at 3 atm. Surplus mechanical energy from the turbine is harnessed to generate electricity through a generator.

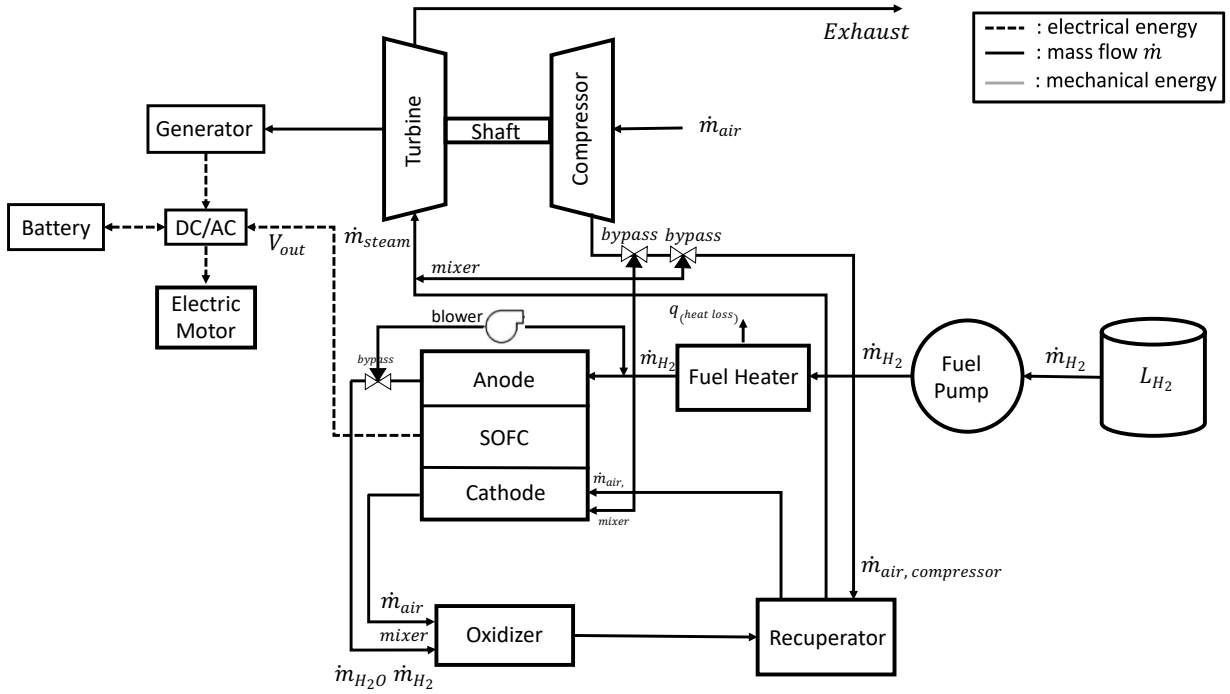

Figure 2: Power train SOFC hybrid for Medium-Range and Long-Range aircraft designed for fuel cell hybrid.

The system was selected for its efficiency and performance enhancements. Integrating the fuel cell (FC) directly, instead of using indirect heating, removes the need for extra heat exchangers. Pressurizing the fuel cell boosts its performance. The system's design, featuring bypasses options and cathode recirculation, facilitates the control of air flow rate and cathode inlet temperature, even at a constant turbine speed. Additionally, air compression not only pre-heats the air but also increases the heat available for the turbine, thereby generating more electricity via a generator.

Pressurizing a Solid Oxide Fuel Cell/Gas Turbine (SOFC/GT) system offers efficiency benefits but raises concerns. Increased pressure can risk cell fracture, especially during rapid pressure changes, and may lead to stall or surge issues in the cathode due to high air volume. To ensure safety, design must choose robust cell materials, use gradual pressure changes, and employ advanced control systems.

A. Static and Dynamic Modeling Governing Equations

The main power source of the proposed system is an SOFC working with hydrogen as fuel (with 2.5 kW/kg and 7.5 kW/kg power densities). The SOFC stack is modeled through a quasi-3-D approach. The stack is divided into five different control volumes, including two bipolar plates, two flow channels, and positive electrode-electrolyte-negative electrode (PEN) assembly. The control volumes are organized in a 5x5 node grid, with each node representing a separate physical process comprising electrochemistry, mass, momentum, and energy conservation, as well as heat and mass exchange inside and between control volumes. In SOFCs, electrochemical reactions concurrently take place on both the cathode and anode sides. Hydrogen is oxidized at the anode, and oxygen is reduced at the cathode. To close the electrical circuit, electrons released during the anodic oxidation reaction move to the cathode through an external wire while oxygen ions (O^{2-}) as a product of the oxygen reduction reaction go through a porous electrolyte to the anode side. These reactions are as follows [19]:

Anodic reaction: $$H_2 + O^{2-} \rightarrow H_2O + 2e^- \quad (1)$$

Cathodic reaction: $$O_2 + 4e^- \rightarrow 2O^{2-} \quad (2)$$

Overall Reaction: $$H_2 + \frac{1}{2} O_2 \rightarrow H_2O \quad (3)$$

Nernst equation is used to calculate the reversible voltage of the SOFC system as follows [20]:

$$V_{rev} = \frac{-\Delta G_0}{nF} + \frac{RT}{nF} \ln\left(\frac{P_{H_2} P_{O_2}^{0.5}}{P_{H_2O}}\right) \quad (4)$$

where ΔG_0 is the Gibbs free energy at standard conditions, n is the number of electrons transferred during the electrochemical reaction, F is Faraday's constant (96485 C/mol e^-), R is the universal gas constant, T is the cell operating temperature, and P is the partial pressure of reacting gases.

It should be noted that SOFCs operation undergoes drops in cell voltage stemming from activation, ohmic, and concentration losses. Therefore, the resulting operating cell voltage will be:

$$V_{cell} = V_{rev} - \eta_{activation} - \eta_{ohmic} - \eta_{concentration} \quad (5)$$

where the voltage drops can be determined following the procedures outlined by McLarty et al. [21]:

Activation losses: $$\eta_{act} = \frac{RT}{\alpha nF} \ln j_0 + \frac{RT}{\alpha nF} \ln j = \frac{2RT}{nF} \sinh^{-1} \frac{j}{2j_0} \quad (6)$$

Ohmic losses: $$\eta_{ohm} = j \times \frac{t_i T}{\sigma_{0,i} e^{-\frac{\Delta G_{act}}{RT}}} \quad (7)$$

$$\eta_{con,a} = -\frac{RT}{nF}\ln\left(\frac{P_{H_2}}{P_{H_2O}}\right)$$

Concentration losses:

$$= -\frac{RT}{2F}\ln\left[\frac{1-\frac{RT}{2F}\frac{jt_a}{D_{a,eff}P_{H_2,in}}}{1+\frac{RT}{2F}\frac{jt_a}{D_{a,eff}P_{H_2O,in}}}\right] \quad (8)$$

$$\eta_{con,c} = -\frac{RT}{nF}ln\left(\frac{P_{O_2}}{P_{O_2,in}}\right)$$

$$= -\frac{RT}{4F}\ln\left[\frac{\frac{P_c}{\delta_{O_2}}-\left(\frac{P_c}{\delta_{O_2}}-P_{O_2,in}\right)\times e^{\frac{RTj\,\delta_{O_2}t_c}{4FD_{c,eff}P_c}}}{P_{O_2,in}}\right] \quad (9)$$

$$\delta_{O_2} = \frac{D_{O_2,k(eff)}}{D_{O_2,k(eff)} + D_{O_{2-N_2},k(eff)}} \quad (10)$$

In above equations, α, j_0, j, t, σ_0, G_{act}, and D denote the charge transfer coefficient (0.5), exchange current density, current density, material thickness, electrical conductivity, activation energy, and diffusivity, respectively.

The SOFC stack power is obtained by multiplying the operating voltage (Equation (5)), current density, the number of cells, and the overall active area of the stack, as shown below:

$$P_{stack} = \frac{V_{cell}\times n\times j\times A}{1000} \quad (11)$$

The current density of a SOFC stack is given by [22]:

$$j = 4\times F\times \dot{n}_{O_2} \quad (12)$$

where $\dot{n}_{O_2}$ is the molar consumption rate of oxygen in the SOFC cathode.

The energy balance for the plates is the balance of multiple ways of heat transfer including convection, conduction, and radiation entering and exiting the plates as follows:

$$m_{plate}C_{plate}\frac{dT}{dt} = Q_{conv} + Q_{cond} + Q_{rad} \quad (13)$$

where m_{plate}, and C_{plate} are the plate mass and heat capacity. Q is the heat transferred.
The energy balance for PEN assembly includes heat generated (Q_{gen}) form the exothermic reaction, as well, which can be given by below equation:

$$\rho VC_{elec}\frac{dT}{dt} = Q_{conv} + Q_{cond} + Q_{rad} + Q_{gen} \quad (14)$$

where ρ, V, C_{elec} denote density, volume, and heat capacity of the electrolyte, respectively. To calculate local convective heat transfer between flows and walls, a fully developed laminar flow and uniform temperature within all control volumes are assumed. Therefore, a constant Nusselt number of four is employed to calculate local convection heat transfer coefficient as in Equation (15):

$$h_c = \frac{Nu_D\, k}{D_h} \tag{15}$$

where h_c is the convective heat transfer coefficient, Nu is the Nusselt number, D_h is the hydraulic diameter, and k is the thermal conductivity.
The energy conservation equations for the flows are calculated by the enthalpy of the inlet and outlet streams as follows:

$$\dot{n}_{air} C_P \frac{dT}{dt} = \dot{n}_{in} h_{in} - \dot{n}_{out} h_{out} + Q_{conv} + Q_{cond} + Q_{rad} - Q_{ion} \tag{16}$$

$$\dot{n}_{fuel} C_P \frac{dT}{dt} = \dot{n}_{in} h_{in} - \dot{n}_{out} h_{out} + Q_{conv} + Q_{cond} + Q_{rad} + Q_{cond} + Q_{ion} - P_{gen} - Q_{gen} \tag{17}$$

In above equations, ṅ, C_p, and h are the molar flow rate, specific heat capacity, and specific enthalpy of the flows in the channels. Q_{ion} shows the heat transferred by oxygen ions, and P_{gen} denotes power generated. The mass balance equations for flow channels are as follows:

$$\dot{n} \frac{dX_i}{dt} = \dot{n}_{in} X_{i,in} - \dot{n}_{out} X_{i,out} + R_{consumed} \tag{18}$$

$$\dot{n}_{fuel} = \frac{I}{2 U_{fuel} F} \tag{19}$$

where X is the molar ratio of reactants, and R is the reaction rate. Equation (19) is used to calculate anode inlet flow rate, in which U_{fuel} is fuel utilization.
Fuel utilization can be determined as follows [23]:

$$U_{fuel} = \frac{\Delta n_{H_2}}{\dot{n}_{H_{2,\,in}}} \tag{20}$$

The overall efficiency of the SOFC stack is calculated as follows [23]:

$$\eta_{overall} = U \times \frac{P_{stack}}{\Delta \dot{H}} \tag{21}$$

where ΔḢ is the difference in the enthalpies of inlet and outlet flows.
The electrochemical efficiency of the cell is determined by the below equation:

$$\eta_{electrochem} = \frac{V_{cell}}{V_{rev}} \tag{22}$$

In the proposed powertrain system, an oxidizer is employed after the SOFC to oxidize the remainder of hydrogen. This configuration can increase the outlet temperature of the SOFC to reach higher temperatures suitable for the turbine performance [24]. The energy balance of the oxidizer is as follows:

$$\dot{n}_{out} C_p \frac{dT}{dt} = \sum \dot{n}_{in} h_{in} - \dot{n}_{out} h_{out} \tag{23}$$

For the compressor and turbine, a dynamic model is employed which includes industry-standard performance maps and dynamic conservation equations. Shaft speed, flow rate, and pressure ratio are normalized as was previously reported by McLarty et al. [24,25]:

$$N_{RPM} = \frac{RPM}{RPM_{des}} \sqrt{\frac{T_{in}}{T_{des}}} \tag{24}$$

$$N_{Flow} = \frac{Flow}{Flow_{des}} \times \frac{\sqrt{\frac{T_{in}}{T_{des}}}}{\frac{P_{in}}{P_{des}}} \tag{25}$$

$$N_{PR} = \frac{P_{out}}{P_{in} PR_{des}} \tag{26}$$

$$PR_{new} = 1 + (PR_{des} - 1) \times \frac{PR_{orig} - 1}{PR_{des,orig} - 1} \tag{27}$$

In the above equations, N is normalized values, PR is the pressure ratio, T_{in} and T_{des} are inlet and design temperatures, and PR_{orig} is the original pressure ratio. The compressor model inputs involve inlet temperature, pressure, and concentrations, shaft speed, and exhaust pressure. Empirical correlations are used to estimate the flow rate into the compressor. Then, compression efficiency is obtained from look-up tables which are based on the normalized speed, flow rate, and pressure. The compressor work is calculated follows the method reported by Lee [24]:

$$\dot{W}_C = \dot{n}_{out} \frac{h_{isen} - h_{in}}{\eta_C} \tag{28}$$

$$\dot{n} C_V \frac{dT_{fluid}}{dt} = \dot{W}_C + \dot{E}_{in} - \dot{E}_{out} + \dot{Q}_{conv} \tag{29}$$

$$\dot{m} C_P \frac{dT_{solid}}{dt} = \dot{Q}_{conv} + \dot{Q}_{rad} \tag{30}$$

where $\dot{W}_C$ is the compressor work, $\dot{n}$ is molar flow rate, $\dot{m}$ is mass flow rate, η_C is compressor efficiency, h_{isen} is isentropic enthalpy, h_{in} is the inlet enthalpy, $\dot{E}_{in}$ and $\dot{E}_{out}$ are energy flows of inlet and outlet, and C_P and C_V are heat capacities.

The turbine model works with inlet temperature, concentrations, inlet flow rate, and exhaust pressure. A control volume method is used to determine the pressure just before the initial turbine stage, which involves a mass balance of the incoming and exhaust flow rates, whereas the scaled

performance map is used to calculate the exhaust flow rate Equation (31). The turbine work is calculated from expansion efficiency and pressure ratio as shown in Equation (32). The energy balance equations are then completed through the inclusion of turbine work and heat transfer between the solid turbine components and the working fluid. These equations are then used to determine the temperatures of the solid metal and fluid exhaust, as shown previously by McLarty et al. And Lee [16,24] via Equations 33 and 34.

$$V\frac{dP}{dt} = (\dot{n}_{in} - \dot{n}_{out})RT_{in} \tag{31}$$

$$\dot{W}_T = \dot{E}_{in} - \dot{n}_{out}(h_{in} - \eta_T(h_{isen} - h_{in})) \tag{32}$$

$$\dot{n}C_V\frac{dT_{fluid}}{dt} = \dot{W}_T + \dot{E}_{in} - \dot{E}_{out} + \dot{Q}_{conv} \tag{33}$$

$$\dot{m}C_P\frac{dT_{solid}}{dt} = \dot{Q}_{conv} + \dot{Q}_{rad} \tag{34}$$

Where V is volume, P is pressure, R is universal gas constant, and $\dot{W}_T$ is turbine work.

B. Initialization and control following Modeling framework.

As depicted in Figure 1 building a model in STRIDES involves initializing and aligning the components assembled in the Plant variable, then steering them towards a steady-state operating condition. This process ensures all variables are appropriately scaled and normalized, mitigating numerical problems, and rounding errors in subsequent computations. Crucially, the states of each component are consolidated into a single vector to be later used in an ordinary differential equation solver. An essential part of this process involves a two-step component initialization, adjusting the model to approximate steady-state operation. The EAGERS user manual has the full guide to how the model is built and run.

The Strides model for an SOFC/GT system involves detailed initialization and control parameters. The initialization function sets fixed component parameters that are independent of inlet values or operational conditions. It also includes an estimate of all states and appropriate scaling factors. The correct choice of these initial values and scales is crucial to ensure system stability. They are stored in a structure that preserves their order throughout the operation of the system. The initialization function also defines the inlet and outlet port names and assigns initial conditions to each. For ports connected to other components, the initial value will be overridden, but for unconnected ports, it remains constant. The initial conditions can also be updated if necessary [17].

Controllers in the Strides model have the same structure and requirements as component functions. They are initialized last, which gives them access to parameters from any of the components. This ordering is important in the context of system linearization, where the controller is left in place to enable the development of optimal MPC (model predicting control) controllers that match the input/output ports of the original controller. In summary, the careful selection of initial values and precise controls is paramount in the Strides model. These choices affect the system's stability and its ability to respond to changes in operational conditions. A more detailed discussion regarding the control's strategy and selection of initial values are to be explored further in the text.

Table 1: Control strategy description

Component	Description
Power Ratio Calculation	Calculate Power Ratio for set points.
Temperature Set Points	Set cathode outlet, cathode inlet, and Turbine Inlet Temperature targets using Power Ratio-dependent linear functions.
RPM Control	Control Revolutions Per Minute using cathode outlet temperature feedback and fuel cell power target feedforward.
Gas Turbine Power Set Point	Determine Gas Turbine power for RPM control, independent of actual output.
Cathode Inlet Temperature Control	Regulate cathode inlet temperature through a bypass valve.
Fuel Cell Power Matching	Align fuel cell power with load demand by adjusting current density.
Temperature Target Adjustment	Modify inlet and outlet temperatures and reduce Turbine Inlet Temperature targets in response to load changes.
Recalibration of Feedforward RPM	Update feedforward Revolutions Per Minute settings by tuning gain and coefficient values.

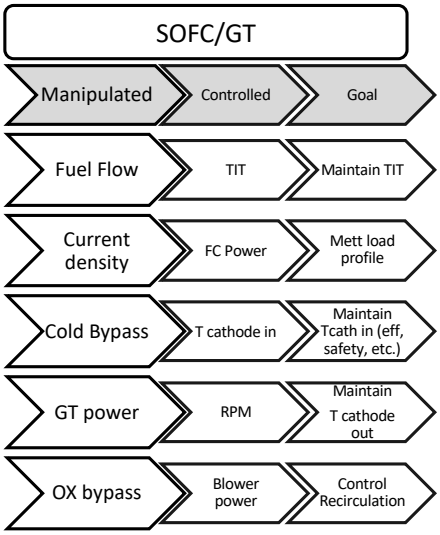

Figure 3: Simplified control strategy for SOFC/GT simulation

In advancing SOFC/GT systems for aeronautical applications, key control strategies, outlined in Figure 3 and Table 1, are crucial. The control strategy is adapted from multiple sources [26,27]. The Power Ratio (PR) sets essential operational parameters, informing linear functions for specific temperature targets: cathode outlet temperature, cathode inlet temperature, and Turbine Inlet Temperature (TIT). RPM control combines feedback from T_{cath_out} and fuel cell power targets with feedforward mechanisms for optimal speed regulation. The Gas Turbine (GT) power set point, vital for RPM stability, operates independently from the GT's actual output. Cathode inlet temperature is regulated through a air bypass valve to maintain ideal thermal conditions. Recuperator Bypass is used to maintain set TIT at 1155k under varying loads, the system adjusts

flow accordingly as changes in load necessitate recalibration of inlet/outlet temperatures and TIT targets for thermal stability. Maintain TIT sustains stability and high efficiency of the turbine and to stay withing limits of the turbine map. Regular recalibration of feedforward RPM settings, involving adjustments in gain and coefficients, refines control accuracy. And finally, oxidizer bypass is used to control recirculation of anode exit using a blower. Strategies collectively optimize the SOFC/GT system for efficient integration into aircraft powertrains.

IV. Demonstration of Dynamic Model on Example Cessna Flight Trajectory

A. Integration analysis

In our previous work [28], we conducted a retrofit analysis for the similarly sized business jet, the Cessna Citation XLS+, which has a cabin volume of approximately 461 ft^3. This was compared to the Cessna S550 Citation S/II, analyzed here, which has a cabin volume of 422 ft^3, excluding baggage storage. Both aircraft are designed to carry 8 passengers. The XLS+ is marginally larger, with about 15% more height and 13% more width than its predecessor. In comparison, as depicted in Table 2, the Cessna Citation S/II offers slightly less spacious cabin dimensions, with a typical length of about 16 feet (4.88 meters), a width of approximately 4.10 feet (1.49 meters), and a cabin height of around 4.9 feet (1.46 meters) [29].

Table 2: Cessna S550 Citation S/II interior dimensions

interior Dimensions	Measurement
Cabin Length	16 feet (4.88 meters)
Cabin Width	4.10 feet (1.49 meters)
Cabin Height	4.9 feet (1.46 meters)
Cabin Volume (excluding baggage)	422 ft^3

However, the primary focus of this paper is not to detail the integration analysis, but rather to demonstrate the feasibility of integrating a SOFC/GT system, following an initial design analysis based on the retrofit methodology developed in our previous work [4]. The Citation S/II is preferred due to its longer range, and lower thrust and power requirements, giving hydrogen aircraft the advantage of a smaller powertrain. The design follows the same approach for tank integration and the SOFC/GT powertrain at the rear of the aircraft.

Table 3: Fuel payload required for max range flight.

Fuel payload for 2000mi		
Jet A	**Hydrogen combustion**	**Hydrogen SOFC/GT**
2,267 kg	815.6 kg	394 kg

As shown in Table 3, the Cessna S/II can carry a maximum fuel payload of 2,267.962 kg, which is equivalent to 815.604 kg of hydrogen for the same flight distance using combustion. Our analysis showed that the SOFC/GT system has an efficiency of approximately 70%, compared to the 34% efficiency of the Pratt & Whitney JT15D-4 turbofan engines. Therefore, for a maximum range flight of 2000 miles, only 394 kg of hydrogen is required. As depicted in Table 4, This initial assessment suggests an integration advantage for SOFC-powered aircraft. Considering the lower thrust and power requirements of approximately 1.3MW for the S/II, the 0.9 MW SOFC analyzed

would weigh 360 kg, the 66 kW gas turbine would weigh 15.4 kg, and the electric motors, based on a density of 7 kW/kg for advanced electric motors, would weigh 182 kg along with cryocoolers (96.8 kg) kg has a power output of 10% of the rated power of aircraft. This setup would replace the two 253 kg JT15D-4 engines, each with a dry weight of 253 kg.

For the system modeled in the dynamic modeling section, the SOFC/GT system is assessed to see its capability of meeting the entire load profile alone without the aid of a battery to help with rapid response. Thus, the SOFC/GT is meeting the entire 1.29 MW power requirement, and no battery is modeled. In the case a battery capable of producing 25% of power rating for 15min, the FC/GT system would only need to provide 75% of the power demand which is 967.5 kW. This second scenario is what is being implemented in the mass analysis above. The aircraft remains well below maximum take-off weight requirements.

Table 4: Mass analysis of retrofitted aircraft

Component	Mass (kg)
MTOW	6849 kg
SOFC System	360
Gas Turbine	15.4
Electric Motors	182
Cryocoolers	96.8
JT15D-4 Turbofan Engine	253 each
Battery	268
Fuel	394
Tanks	78
Total takeoff mass	5,953<MTOW

The SOFC unit would occupy a volume of approximately 5.65 cubic feet, while the gas turbine would occupy around 0.09 ft^3. Given that the standard Cessna S/II has a cabin volume of 422 cubic feet excluding baggage storage, the SOFC system would take up about 1.34% (56.6 ft3) of the cabin volume in block shaped setup, the GT 0.09025 ft^3, the battery if sized to 322kw power output and 80.63 kWh, would occupy a volume of 4.25 ft^3 considering a power and an energy density of 0.67 kWh/L. The volume analysis indicated the powertrain system can fit in the back of the aircraft whilst remaining within the center of gravity envelope.

B. Implementation Analysis:

To assess the viability of integrating a SOFC engine into a conventional aircraft, a demonstration of the dynamic model on an example existing subsonic business jet configuration was utilized. In this model, all the technical specifications of the Cessna S550 Citation S/II were retained, with the sole modification being the replacement of the jet engines, and a retrofit with SOFC engines.

To demonstrate the dynamic modeling, a representative thrust profile of an observed trajectory of this aircraft from surveillance data was modeled. The observed trajectory selected was a flight from Dulles International Airport (IAD) to Cyril E. King Airport (STT) of an existing Cessna S550

Citation S/II obtained from FlightRadar24, as depicted in Figure 4 [30]. The required percentage of maximum thrust per time of the retrofit SOFC engine for the chosen flight trajectory was determined using a low fidelity performance model of the aircraft under the conditions shown in Table 5. This necessitated the determination of the drag and lift profile, weight distribution profile, distance traveled, and altitude of the flight trajectory.

Table 5: Flight conditions for example flight trajectory of Cessna S550 Citation S/II from Dulles International Airport (IAD) to Cyril E. King Airport (STT)

Parameters	***Values***
Maximum take off weight (lbs)	15,100
Range (nmi)	1551
Takeoff Field Length (ft)	10,501
Cruise Mach Number	0.67
Cruise Altitude (ft)	42,950
Pressure at Cruise Altitude (atm)	0.16
Temperature at Cruise Altitude ($°R$)	389.97

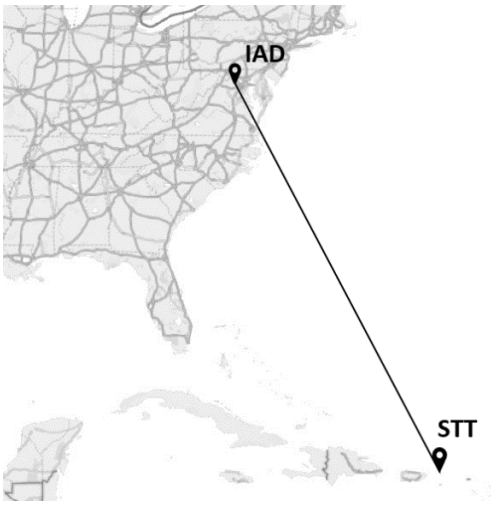

Figure 4: Example flight trajectory of Cessna S550 Citation S/II from Dulles International Airport (IAD) to Cyril E. King Airport (STT)

This preliminary analysis was conducted by utilizing FlightRadar 24 for coordinates and velocity profile acquisitions for subsequent calculations. It is pertinent to note that only ground speed was available for this analysis and thus was the speed used in the performance model for simplicity; however, since this trajectory is just for demonstration, it is believed that this is sufficient for the dynamic modeling demonstration. The thrust profile is contingent upon the weight of the aircraft of each segment, the climb or descent angle if the aircraft is in the climb or approach phase of the trajectory, and the aerodynamic efficiency. Assuming a point mass model of the aircraft, the thrust was modeled for each timestamp of the flight trajectory using the following equation:

$$T = w\left(\sin(\gamma) + \frac{1}{\frac{L}{D}}\right) \tag{35}$$

By using the great circle distance equation, along with the longitude and latitude coordinates of the flight trajectory, the altitude, distance traveled by the aircraft, and flight path angle (γ) can be easily obtained. To acquire the thrust needed per each flight segment, the weight of the aircraft was determined using the Breguet Range Equation over incremental segments of the flight:

$$w_{fuel} = \frac{w_{initial}}{e^{u}} \; ; \; u = \frac{R \cdot g}{\frac{L}{D}\eta h_f} \tag{36}$$

Where r and g represent the range of the flight and gravitational force, respectively. In addition, the weight variation using the SOFC engine is found to be minimal. This is due to the power efficiency and fuel consumption of liquid hydrogen. Kerosene has a specific energy of 43MJ/kg while liquid oxygen has roughly a specific energy of 120MJ/kg. This, in turn, lowers the fuel weight carried by the aircraft by 25%. However, this will raise a new challenge for the fuel tanks, as later discussed in the conclusion section.

To obtain the thrust profile, drag must also be calculated using temperature, Mach number, pressure, and density at a specific altitude. This is important as both the parasite drag, and induced drag takes in density and the Reynolds number. Drag, depicted in Figure 5, can then be calculated using the equation below:

$$D = \frac{1}{2}\rho v^2 S_{ref} \cdot \left(C_{D_c} + C_{D_o} + C_{D_{gear}} + C_{D_I}\right) \tag{37}$$

Where the compressibility drag coefficient is only accounted for during the cruise phase. Additionally, the landing gears are deployed only during takeoff, approach, and landing operations of the flight trajectory.

Figure 4 above recreates the flight trajectory, flying from IAD to STT, by utilizing the longitude and latitude coordinates retrieved from the flight tracking website FlightRadar24 [30]. The result acquired from Eq. (35) is illustrated in Figure 6**,** showing the changes in maximum thrust needed for the takeoff, climb, cruise, approach, and landing phases. From the graph, it is observable that the thrust needed for the cruise phase is approximately 22%. This aligns closely with what typically is required for a Boeing737-800[31]. The landing phase of the trajectory exhibits significantly higher thrust requirements due to factors such as reversed thrust, deployed landing gear, and flaps. This methodology was examined for multiple flight trajectories to study the sturdiness and resilience of the dynamic model. The results of additional flight paths, demonstrated on the same Cessna S550 Citation S/II flying from Cyril E. King Airport (STT) to Treasure Coast International Airport (FPR), can be found in Figure A-C**.**

For dynamic modeling, the power demand illustrated in this profile will be pivotal. However, recognizing the potential variability in real-world scenarios, we will also investigate rougher mission profiles with challenging conditions such as adverse weather and high turbulence. The profile will be adapted accordingly to reflect these variables. Moreover, the system's ability to deliver the necessary power even in the event of a propulsion unit failure is important for safety during critical flight stages such as take-off or climb. Guided by the FAA's airworthiness standard

(§23.21220) [32], a minimum power requirement of is derived to ensure a climb gradient of 2% under a One Engine Inoperative (OEI) scenario at Second Segment Climb (SSC).

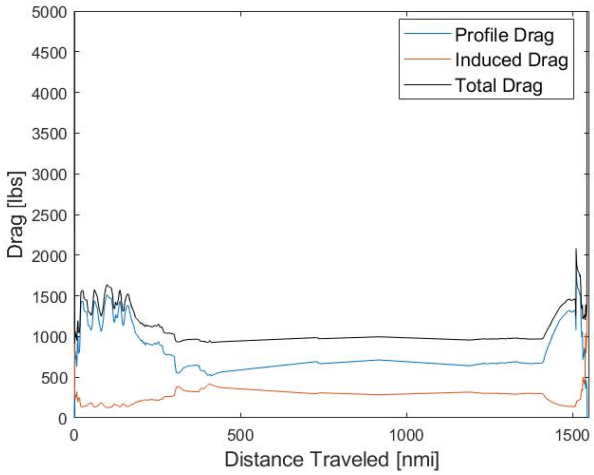

Figure 5: Aircraft drag profile of the example Cessna S550 Citation S/II flight trajectory.

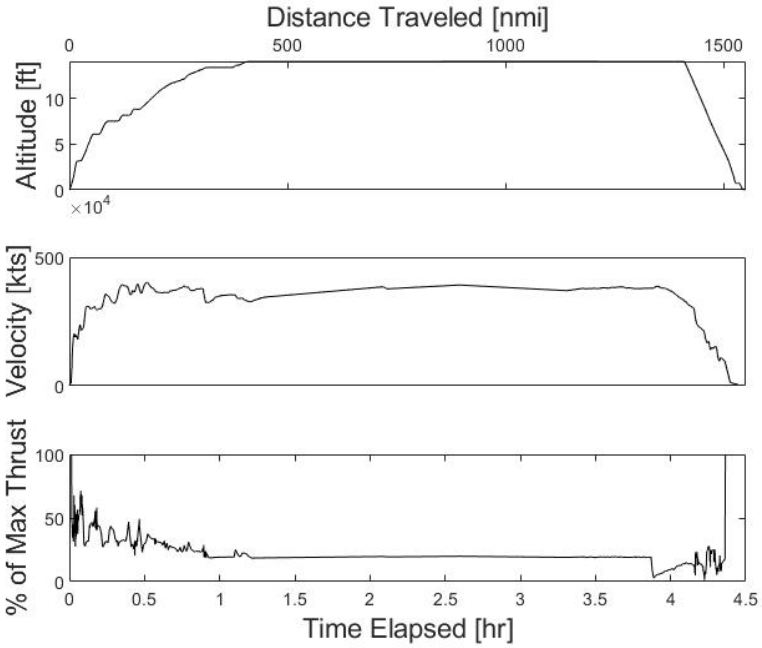

Figure 6: Aircraft altitude, velocity, and modeled percentage of maximum thrust versus distance traveled and time of the example Cessna S550 Citation S/II flight trajectory.

C. Static Modeling

The stack is discretized into five control volumes; two bipolar plates, two flow channels and positive electrode-electrolyte-negative electrode (PEN) assembly. Table 6 portrays some properties of the stack/cell. The stack/cell model key assumptions include treating gases as ideal due to operating conditions, unidirectional electrical current flow, instantaneous electrochemical reactions, and uniform gas distribution across channels. Each gas node functions as a Continuously Stirred Tank Reactor, and a lumped temperature approach is adopted for the cell's solid structure. The model assumes adiabatic boundaries at cell inlets and outlets, high electrical conductivity with isopotential surfaces for electrodes and collectors, a constant Nusselt number, and laminar flow regimes in both cathode and anode streams. Lastly, it disregards external heat losses. These assumptions streamline the model, focusing on internal dynamics, though they might limit real-world applicability under varying conditions[33].

Table 6: Thermal and physical properties of SOFC components

Properties	Value
Electrolyte conductivity	6.19 W/m·K
Membrane thickness	5e-6 m
Cathode thickness	295e-6 m
Anode thickness	50e-6 m
SOFC diameter	0.02025 m
SOFC length	0.040 m
Number of cells per kW	27

The system is pressurized at 3 atm. It assumes an ambient pressure of 1 atm, which is an aspect to improve in the future. This is likely to cause a slight decrease in efficiency, for instance, if we were to start at 0.5 atm, a factor not accounted for. The stack is designed to operate with an inlet temperature of 998 K, and a turbine inlet temperature of 1155 K. The topping cycle benefits from operating on hydrogen, where the reaction in the PEN is exothermic, without any endothermic reforming that reduces temperature. This, however, raises additional concerns regarding thermal management and degradation of the cell and control complexities. The average temperature across the PEN was 1190 K, increasing the ΔT_{PEN} and thus reducing the maximum thermal gradient.

D. Dynamic Modeling

In Figure 7, the transient simulation results are presented for both the compressor and turbine operating points. For the turbine, the operational data points are suitably located within a high-efficiency region, maintaining a safe distance from the choke line, which signifies optimal performance without approaching the flow capacity limit. Likewise, the compressor's operational points are strategically positioned in a zone of high efficiency, well clear of the surge lines, thus preventing the risk of operational instability or reverse flow phenomena.

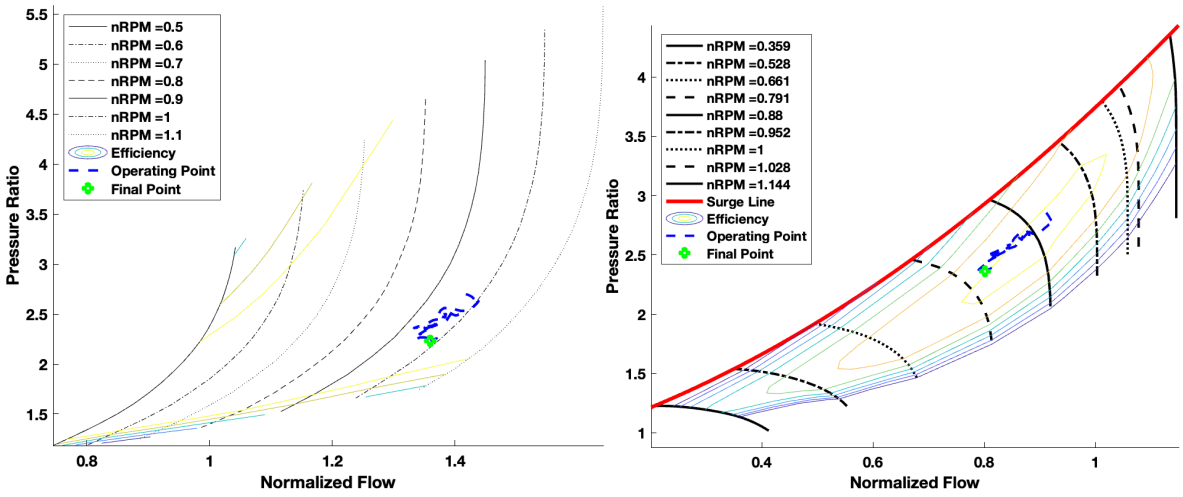

A) B)

Figure 7: operation point through our simulation of A) turbine. B) Compressor

Figure 8 depicts the operational efficiency of the compressor and turbine throughout the simulation. As anticipated, the compressor exhibits relatively consistent efficiency characteristics, as reflected in the simulation results in response to varying power demands. In contrast, turbine efficiency demonstrates a slightly greater degree of sensitivity. The turbine efficiency exhibits a gradual and minor decline before stabilizing at a negligible level of decrease.

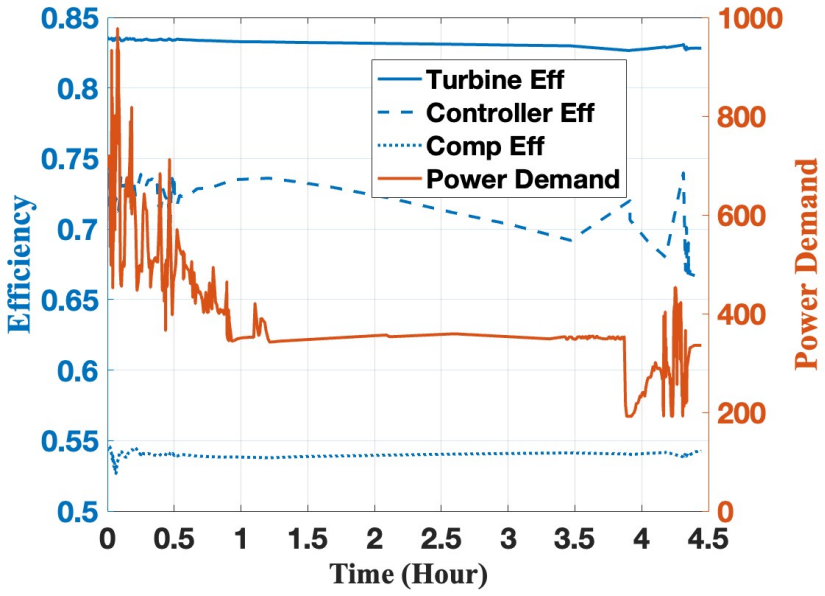

Figure 8: Efficiency Curves & Power Demand

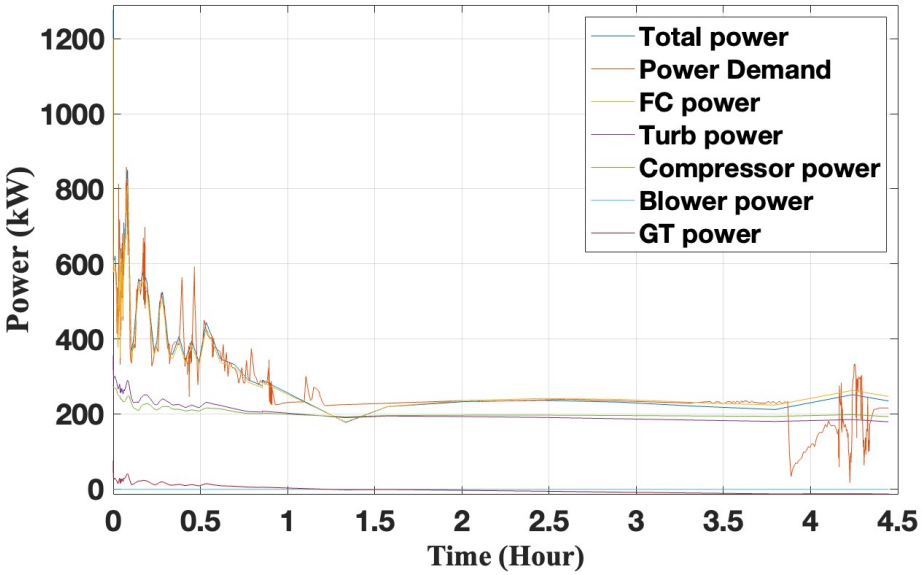

Figure 9: Power demand vs Power of components

From a technical standpoint, it is discernible that while SOFC/GT systems are lauded for their efficiency and reduced environmental footprint, their aptitude in swiftly responding to load variations, especially at higher operational magnitudes, remains a pivotal area for enhancement. The empirical evidence suggests a more agile response in smaller-scale systems, exemplified by Kandepu et al. finding of a 40% load change being managed within a mere 5-second window in a 278-kW system [34]. In contrast, larger systems exhibit notably slower response times, as highlighted by Ahrned et al., [35] where a substantial system with a similar sized system of 1150kw by Brouwer et al showed 43,200 seconds for a 17.46% turndown and an equal value for ramp up. This enhanced responsiveness in smaller systems is likely due to the reduced thermal mass and less complex system dynamics. The contrast between these examples underscores the variability in response times across different scales of SOFC/GT systems.

Upon successful completion of the static modeling and the generation of test profiles, the control strategy for the SOFC/GT system was iteratively refined to achieve optimal response to the varying power demands of different mission profiles. It was observed that each profile elicited a distinct reaction from the control mechanisms. This included the profile detailed in the implementation analysis section. Broadly, the system demonstrated proficiency in managing the majority of scenarios, barring extreme conditions of rapid power escalation (ramp-up) and reduction (turndown). The FC did most of the heavy lifting of power output whilst the GT contributed about 95 kW of electric power (via generator) in the begging of the flight and gradually decreased likely due to the increasing requirement of the compressor.

Specifically, for the profile depicted in Figure 9, the SOFC/GT system exhibited a robust response to the power demands. During instances of exceptionally swift power turndown (less than 60 seconds), the system maintained a consistent power output. Total Power Demand shows a peak at the beginning, indicating a surge in power requirement, which then stabilizes and gradually declines over the period. Power Output from Fuel Cells (FC) demonstrates a sharp increase initially

and then stabilizes at a lower value compared to the peak of total power demand, suggesting that fuel cells respond to initial demand but do not match the total demand alone within the noticeably short ramp up and down times. Notably, the system maintained an output close to the cruising level even during rapid power variations in the descent phase. Overall, the system displayed good rapid response capabilities and an aptitude for adapting to the dynamic requirements of flight. However, during the last 1 hour of flight, the system overpowers the demand by ~14% of data points.

Moreover, a second flight profile was also assessed (details available in the Appendix). This profile experienced a very sudden increase to maximum throttle in the last minutes, likely due to the landing conditions. The implementation of the control strategy appeared to react differently based on multiple factors. Most notably, if the system is unable to cope with rapid fluctuations in demand throughout the profile, it sets the total power demand slightly higher to remain on the positive side of the fluctuation. Now, if a battery is integrated to power 25% of the aircraft, this kind of increase in energy could be stored in the battery. Furthermore, the battery itself has a semi-instantaneous discharge capacity, which has been proven in practice and in the literature to be capable of managing such dynamics, and even more complex scenarios.

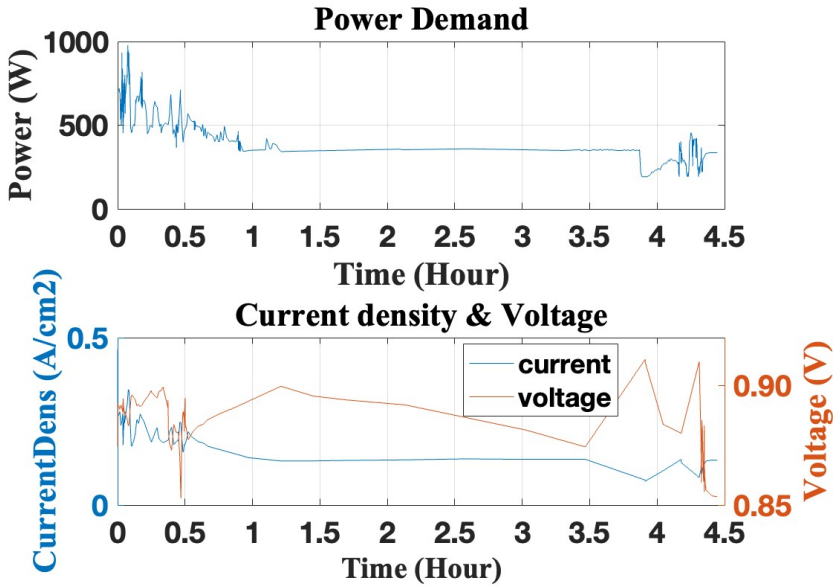

Figure 10: Current density & voltage

The SOFC/GT system demonstrated remarkable efficiency, achieving an efficiency of 71.4%, a testament to its promising potential for aviation applications. However, this efficiency declines during the latter stages of the flight, particularly under conditions of high dynamic stress. This observed decrease in efficiency can be attributed to several factors, including increased polarization losses due to heightened current densities and variations in reactant concentrations under dynamic operating conditions. In terms of specific operational parameters, the dynamic model of the SOFC/GT system for aviation applications encompassed 36,300 cells, indicating a substantial size for robust power generation, with an average power output of 34 W/cell. Depicted

in Figure 10, The average cell voltage was maintained at 0.86 volts, and the current density at 0.22 A/cm^2, is on the lower end of the spectrum (0.2 to 1.5 A/cm²) of operation most likely due to operating under low partial load conditions. You see current densities of around 0.46 A/cm^2 at the beginning of the flight when higher power is required.

During the turbulent descent phase of the aircraft, as observed in our mission profile analysis, the synergy between the battery and the SOFC/GT system proved crucial. The battery efficiently managed rapid power fluctuations, providing immediate energy support and stability. This integration was essential in maintaining continuous, stable power supply and reducing stress on the fuel cells, thereby ensuring the aircraft's safe and efficient operation during this critical phase. Incorporating a battery into the SOFC/GT system significantly bolsters its performance, especially in managing transient loads. The battery serves as an energy buffer, capable of instantaneously delivering or absorbing power. This is crucial in aviation applications where power fluctuations can be abrupt and frequent. The battery's high-power density, ranging from 0.265 kW/kg, enables it to respond swiftly to these demands, ensuring system stability during rapid power changes.

For example, in scenarios where the SOFC/GT system experiences a rapid 20% power ramp-up, the battery can instantaneously supply up to 40% of the needed power. This rapid response is vital for maintaining the SOFC operating temperature within its optimal range, which is essential for efficient fuel utilization and extended cell lifespan. The addition of a battery also significantly reduces the cyclical stress on the fuel cells, leading to a 30-40% decrease in thermal and mechanical stress. Furthermore, a battery with a capacity of around 200 kWh increases the system's operational flexibility. This capacity allows the system to handle transient loads for up to 15 minutes under an average transient power demand of 800 kW. Such capability is particularly crucial during critical flight phases like takeoff and landing. Overall, the integration of a battery not only improves the SOFC/GT system's responsiveness but also enhances its overall efficiency, typically by 5-10% during dynamic flight conditions. This improvement is a testament to the synergy between the battery and the SOFC/GT system in meeting the demanding energy requirements of aviation applications.

V.Summary and Conclusion

In summary, the presented study of retrofitting an existing business jet with SOFC engines underscores the potential and challenges of this innovative technology in aviation. Our low-fidelity analysis of a typical flight profile demonstrated the dynamic capabilities of the SOFC/GT system, achieving an efficiency of 71.4%. This robust power generation capacity and rapid response to varying power demands highlight the system's dynamic operating adaptability and practicality for aviation applications.

However, the study also revealed some critical areas for further development. The overpowering observed during the final hour of flight and the decline in efficiency under dynamic conditions suggest the need for further optimization of the system. The integration of a battery with the SOFC/GT system emerged as a significant enhancement, providing a buffer for power fluctuations, and reducing stress on the fuel cells, thereby improving overall efficiency and responsiveness.

Future comprehensive analyses using advanced aircraft optimization tools like SUAVE are essential. These should focus on the aircraft performance with the new engines and delve into the challenges posed by using liquid hydrogen as a fuel source. The control of temperature with cryogenic fuel storage necessitates advanced temperature-controlled fuel tanks, demanding careful examination of the materials, volume, and design of these tanks. The potential impacts on the size, weight, and structural design of the aircraft, as well as the placement of the cryogenic tanks for stability, require thorough investigation.

The retrofitting analysis of a hydrogen aircraft further demonstrated that while the integration of tanks and powertrain is feasible within the cabin, it results in significant trade-offs, such as the loss of approximately half the passenger seating for the maximum rated range flight. Additionally, the mass analysis indicated that a retrofitted SOFC/GT/Battery aircraft would remain well within the maximum take-off weight limits, underscoring the practicality of this approach.

In summary, while the initial results are promising, highlighting the SOFC/GT system's efficiency and dynamic operating adaptability, but the need for a battery capable of 15-25% of power output is emphasized. Significant research and development efforts are needed to address these challenges and others to advance the system for practical aviation use. As the industry moves towards more sustainable and efficient energy sources, the advancements in SOFC technology and its integration with energy storage solutions offer a promising avenue for the future of aviation.

VI.Appendix

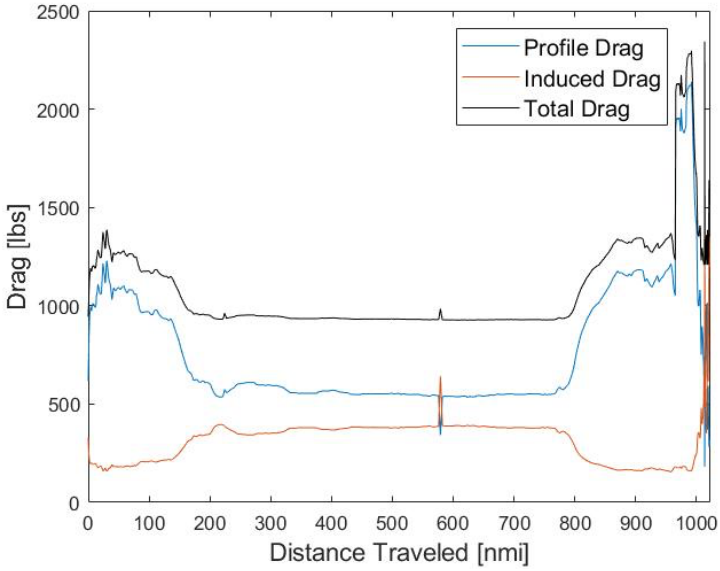

Figure A: Aircraft drag profile of the example Cessna S550 Citation S/II flight trajectory

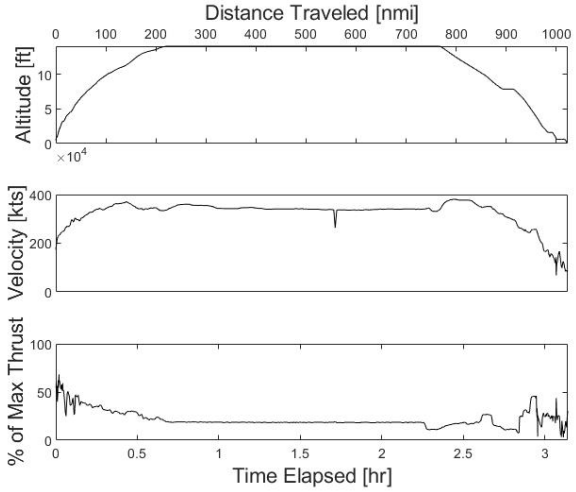

Figure B: Aircraft altitude, velocity, and modeled percentage of maximum thrust versus distance traveled and time of the example Cessna S550 Citation S/II flight trajectory.

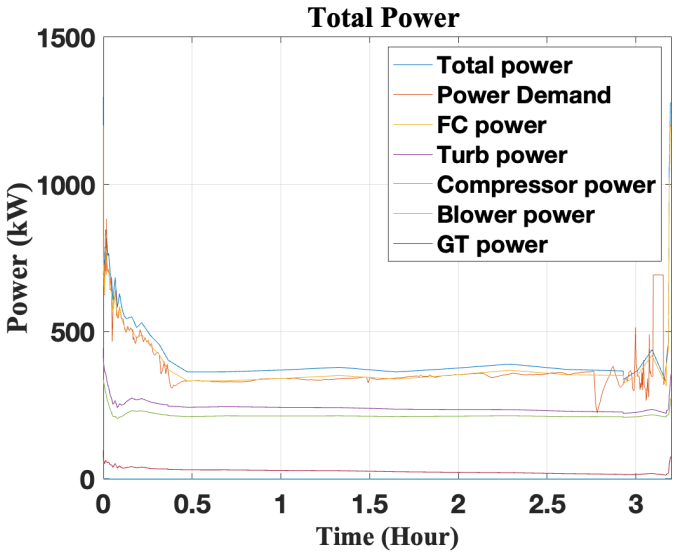

Figure C: Power profile for second mission profile analyzed.

VII.Acknowledgments

Our sincere gratitude is extended to the developers of the STRIDES platform and the architects of the components modified for our dynamic modeling efforts, including Prof. Dustin McLarty, Dr. Alireza Saeedmanesh, Dr. GJ Lee, Prof. Scott Samuelsen, and Prof. Jack Brouwer.

VIII.References

[1] Terrenoire, E., Hauglustaine, D. A., Gasser, T., and Penanhoat, O., "The Contribution of Carbon Dioxide Emissions from the Aviation Sector to Future Climate Change," *Environmental research letters*, Vol. 14, No. 8, 2019, p. 084019.

[2] Chakravarthula, V. A., Roberts, R. A., and Wolff, M., "Dynamic Model of Solid Oxide Fuel Cell Integrated with Fan and Exhaust Nozzle," 2016. https://doi.org/10.2514/6.2016-4718

[3] Collins, J. M., and McLarty, D., "All-Electric Commercial Aviation with Solid Oxide Fuel Cell-Gas Turbine-Battery Hybrids," *Applied Energy*, Vol. 265, 2020, p. 114787.

[4] Alsamri, K., De la Cruz, J. J., Emmanouilidi, M., Huynh, J. L., and Brouwer, J., "Correction: Methodology to Assess Emissions and Performance Trade-Offs for a Retrofitted Solid Oxide Fuel Cell Hybrid and Hydrogen Powered Aircraft," 2023.

[5] FAA, "Title 14 - Aeronautics and Space Parts 1 - 1399. January 1, 2023."

[6] Rossi, I., Traverso, A., and Tucker, D., "SOFC/Gas Turbine Hybrid System: A Simplified Framework for Dynamic Simulation," *Applied energy*, Vol. 238, 2019, pp. 1543–1550.

[7] Roberts, R. A., and Brouwer, J., "Dynamic Simulation of a Pressurized 220kW Solid Oxide Fuel-Cell–Gas-Turbine Hybrid System: Modeled Performance Compared to Measured Results," 2006.

[8] Mueller, F., Jabbari, F., Brouwer, J., Roberts, R., Junker, T., and Ghezel-Ayagh, H., "Control Design for a Bottoming Solid Oxide Fuel Cell Gas Turbine Hybrid System," 2007.

[9] Glnaz Pourabedin, "Dynamic Modeling of Planar Solid Oxide Fuel Cell System for Regional Jet Aircraft Application (Simple System)," *International Journal of Modern Studies in Mechanical Engineering*, Vol. 4, No. 2, 2018. https://doi.org/10.20431/2454-9711.0402003

[10] Chakravarthula, V. A., "Transient Analysis of a Solid Oxide Fuel Cell/ Gas Turbine Hybrid System for Distributed Electric Propulsion."

[11] Litt, J., Frederick, D., and Guo, T.-H., "The Case for Intelligent Propulsion Control for Fast Engine Response," 2009.

[12] Merrill, W., Tran Van, H., and Mink, G., "Fast Engine Response for Emergency Aircraft Operation," *AIAA Infotech@ Aerospace 2010*, 2010, p. 3491.

[13] Zhang, B., Maloney, D., Farida Harun, N., Zhou, N., Pezzini, P., Medam, A., Hovsapian, R., Bayham, S., and Tucker, D., "Rapid Load Transition for Integrated Solid Oxide Fuel Cell – Gas Turbine (SOFC-GT) Energy Systems: A Demonstration of the Potential for Grid Response," *Energy Conversion and Management*, Vol. 258, 2022, p. 115544. https://doi.org/10.1016/j.enconman.2022.115544

[14] Ahrend, P. N., "Solid Oxide Fuel Cell Hybrid Systems for Dynamic Rail Applications," University of California, Irvine, 2020.

[15] Ferrari, M. L., Rossi, I., Sorce, A., and Massardo, A. F., "Advanced Control System for Grid-Connected SOFC Hybrid Plants: Experimental Verification in Cyber-Physical Mode," *Journal of Engineering for Gas Turbines and Power*, Vol. 141, No. 9, 2019, p. 091019.

[16] McLarty, D. F., “Fuel Cell Gas Turbine Hybrid Design, Control, and Performance,” University of California, Irvine, 2010.
[17] McLarty D, Jones N, Mikeska H, Mills A, and Panossian N, “The Efficient Allocation of Grid Energy Resources Including Storage (EAGERS),” 2018. Retrieved 7 September 2023. https://github.com/ CESI-Lab/EAGERS.
[18] Alsamri, K., De la Cruz, J. J., Emmanouilidi, M., Huynh, J. L., and Brouwer, J., “Correction: Methodology to Assess Emissions and Performance Trade-Offs for a Retrofitted Solid Oxide Fuel Cell Hybrid and Hydrogen Powered Aircraft,” 2023.
[19] Ormerod, R. M., “Solid Oxide Fuel Cells,” *Chemical Society Reviews*, Vol. 32, No. 1, 2003, pp. 17–28.
[20] Dicks, A. L., and Rand, D. A. J., “Fuel Cell Systems Explained,” John Wiley & Sons, 2018.
[21] McLarty, D., Brouwer, J., and Samuelsen, S., “A Spatially Resolved Physical Model for Transient System Analysis of High Temperature Fuel Cells,” *international journal of hydrogen energy*, Vol. 38, No. 19, 2013, pp. 7935–7946.
[22] Wilson, J. A., Wang, Y., Carroll, J., Raush, J., Arkenberg, G., Dogdibegovic, E., Swartz, S., Daggett, D., Singhal, S., and Zhou, X.-D., “Hybrid Solid Oxide Fuel Cell/Gas Turbine Model Development for Electric Aviation,” *Energies*, Vol. 15, No. 8, 2022, p. 2885. https://doi.org/10.3390/en15082885
[23] Freeh, J. E., Pratt, J. W., and Brouwer, J., “Development of a Solid-Oxide Fuel Cell/Gas Turbine Hybrid System Model for Aerospace Applications,” Vol. 41723, 2004, pp. 371–379.
[24] Lee, G. J., “More Efficient Dynamic Operation of Fueled Dispatchable Power Generation in a High Renewable Penetration Grid,” University of California, Irvine, 2022.
[25] McLarty, D., Brouwer, J., and Samuelsen, S., “Hybrid Fuel Cell Gas Turbine System Design and Optimization,” *Journal of Fuel Cell Science and Technology*, Vol. 10, No. 4, 2013, p. 041005.
[26] McLarty, D., Brouwer, J., and Samuelsen, S., “Fuel Cell–Gas Turbine Hybrid System Design Part II: Dynamics and Control,” *Journal of Power Sources*, Vol. 254, 2014, pp. 126–136. https://doi.org/10.1016/j.jpowsour.2013.11.123
[27] Lee, G. J., and Brouwer, J., “More Efficient Dynamic Operation of Fueled Dispatchable Power Generation in a High Renewable Penetration Grid,” United States -- California, 2022.
[28] Alsamri, K., De la Cruz, J. J., Emmanouilidi, M., Huynh, J. L., and Brouwer, J., “Methodology to Assess Emissions and Performance Trade-Offs for a Retrofitted Solid Oxide Fuel Cell Hybrid and Hydrogen Powered Aircraft,” 2023.
[29] Jane, F. T. (Frederick T., “Jane’s All the World’s Aircraft.,” *Jane’s all the world’s aircraft.*, 1909.
[30] “Flight Radar 24.” Retrieved 27 November 2023. https://www.flightradar24.com/data/aircraft/n550we#32fc8cee
[31] FAA, “2022-03967.” Retrieved 11 November 2023. https://www.federalregister.gov/d/2022-03967
[32] Kammermann, J., Bolvashenkov, I., Tran, K., Herzog, H.-G., and Frenkel, I., “Feasibility Study for a Full-Electric Aircraft Considering Weight, Volume, and Reliability Requirements,” 2020.

[33] Saeedmanesh, A., Colombo, P., McLarty, D., and Brouwer, J., "Dynamic Behavior of a Solid Oxide Steam Electrolyzer System Using Transient Photovoltaic Generated Power for Renewable Hydrogen Production," *Journal of Electrochemical Energy Conversion and Storage*, Vol. 16, No. 4, 2019. https://doi.org/10.1115/1.4043340
[34] Kandepu, R., Imsland, L., Foss, B. A., Stiller, C., Thorud, B., and Bolland, O., "Modeling and Control of a SOFC-GT-Based Autonomous Power System," *Energy*, Vol. 32, No. 4, 2007, pp. 406–417. https://doi.org/10.1016/j.energy.2006.07.034
[35] Brouwer, J., "Hybrid Gas Turbine Fuel Cell Systems," 2003.